LETTERS

Thermochemical flows couple the Earth's inner core growth to mantle heterogeneity

Julien Aubert[1], Hagay Amit[2], Gauthier Hulot[2] & Peter Olson[3]

Seismic waves sampling the top 100 km of the Earth's inner core reveal that the eastern hemisphere (40° E–180° E) is seismically faster[1,2], more isotropic[2,3] and more attenuating[4] than the western hemisphere. The origin of this hemispherical dichotomy is a challenging problem for our understanding of the Earth as a system of dynamically coupled layers. Previously, laboratory experiments have established that thermal control from the lower mantle can drastically affect fluid flow in the outer core[5], which in turn can induce textural heterogeneity on the inner core solidification front[6]. The resulting texture should be consistent with other expected manifestations of thermal mantle control on the geodynamo, specifically magnetic flux concentrations[7,8] in the time-average palaeomagnetic field[9,10] over the past 5 Myr, and preferred eddy locations[11] in flows imaged below the core–mantle boundary by the analysis of historical geomagnetic secular variation[12]. Here we show that a single model of thermochemical convection and dynamo action can account for all these effects by producing a large-scale, long-term outer core flow that couples the heterogeneity of the inner core with that of the lower mantle. The main feature of this thermochemical 'wind' is a cyclonic circulation below Asia, which concentrates magnetic field on the core–mantle boundary at the observed location and locally agrees with core flow images. This wind also causes anomalously high rates of light element release in the eastern hemisphere of the inner core boundary, suggesting that lateral seismic anomalies at the top of the inner core result from mantle-induced variations in its freezing rate.

In the lower mantle, the double crossing of the post-perovskite phase transition detected by core-reflected seismic shear waves[13] directly constrains local temperature gradients. Heat flow from the core to the mantle is found[14] to be larger than average below Central America, where descending mantle currents induce regional heat flow anomalies of $\delta q = 40\ \mathrm{mW\ m^{-2}}$ or larger, and lower than average below the central Pacific. These results support a thermal interpretation of the largest scales present in seismic shear velocity maps[15], according to which fast regions correspond to cold deep subducted lithosphere[14,16] (as beneath Central America), and extract more heat from the core, while slow regions correspond to warm thermochemical piles[17,18] (as beneath the central Pacific), and extract less heat from the core. Cooling causes the inner core to grow at nominal rates of 0.3–0.9 mm $\mathrm{yr^{-1}}$ (ref. 19), corresponding to 100 km of solidification within the past 100–300 Myr. As the large-scale lower mantle structure has changed little during that time[18], a connection between its present-day pattern and the upper inner core heterogeneous properties is plausible.

The following numerical simulation shows how thermal mantle heterogeneity simultaneously affects the time-average outer core magnetic field structure, core flow, and the asymmetric structure of the inner core. We use the same model of Boussinesq convection and dynamo action in a rotating spherical shell as in a previous study[11], except for the use of a co-density formulation[20] to describe both thermal and chemical buoyancy sources in the outer core in terms of a single co-density variable C (see Methods). We assume that the thermal and chemical perturbations have the same effective diffusivity κ because of turbulent mixing. At the core–mantle boundary, we assume zero chemical mass flux, so the mass anomaly flux $f = -\kappa \partial C/\partial r$ there (which combines thermal and chemical contributions) is related to the heat flow q through $f = \alpha q/C_p$, where r is the radial coordinate, and α and C_p are respectively the thermal expansivity and the specific heat of the liquid outer core. Thermal mantle control is modelled by imposing a heterogeneous heat flow pattern proportional to lowermost mantle seismic shear velocity anomalies[15] (Supplementary Fig. 1), superimposed on a uniform background heat flow, as in earlier studies[7,8]. The seismically inferred amplitude[13,14] $\delta q = 40\ \mathrm{mW\ m^{-2}}$ of the lateral heat flow variation corresponds to a mass anomaly flux variation $\delta f = 5 \times 10^{-10}\ \mathrm{kg\ m^{-2}\ s^{-1}}$, using[21] $\alpha = 10^{-5}\ \mathrm{K^{-1}}$ and $C_p = 800\ \mathrm{J\ kg^{-1}\ K^{-1}}$. This is of the same order of magnitude as the estimated homogeneous part of the mass anomaly flux in the core[21] $f_o = 2 \times 10^{-10}\ \mathrm{kg\ m^{-2}\ s^{-1}}$, expressed per unit surface at the core–mantle boundary. Accordingly, we specify $\delta f/f_o = 1$ in our model. At the inner core boundary, the co-density C is set to a constant value, and f is free to react to the convection. This thermodynamically consistent boundary condition (see Supplementary Information) allows for a spatially variable release of heat and light elements, and implies[20] lateral variations in the inner core growth rate, which is fastest where outer core downwellings bring relatively cold and chemically depleted liquid close to the inner core boundary. The simulation parameters are chosen so that the model produces a self-sustained magnetic field with dipole reversals. Because of the great disparity in the timescales of outer core and mantle dynamical processes, we consider only the time-average behaviour of the model. The flow is then dominated by a thermochemical wind balance[11] between the pressure gradient and the Coriolis and buoyancy forces.

The most prominent non-axisymmetric feature of the resulting thermochemical wind (Fig. 1) is a cyclonic (anticlockwise on a north polar view) flow column, parallel to the rotation axis, extending from the outer to the inner boundary, just outside the inner core tangent cylinder. The column is located below Asia, and is driven by mantle-induced lateral temperature gradients between the cold sub-Asian region and warmer African and Pacific regions. Two additional columns are located below the Pacific and Atlantic oceans. Strong helical polar vortices are generated inside the northern and southern parts of the tangent cylinder. The Asian cyclone is visible in the flow at the top of the free stream (Fig. 2d), and locally concentrates[22] the outer boundary radial magnetic field (Fig. 2b). Similar signatures are found

[1]Dynamique des Fluides Géologiques, [2]Géomagnétisme, Institut de Physique du Globe de Paris, Université Paris-Diderot, INSU/CNRS, 4, Place Jussieu, 75252, Paris cedex 05, France. [3]Department of Earth and Planetary Sciences, Johns Hopkins University, Baltimore, Maryland 21218, USA.

in the time-average core flow (Fig. 2c) and palaeomagnetic field (Fig. 2a), showing that these patterns could indeed result from the presence of such a cyclone in the Earth's outer core. Our model (Fig. 2b, d) further shows that the second persistent palaeomagnetic flux lobe below north America (Fig. 2a) is associated with a similar long-term cyclone, suggesting that the anticyclonic flow inferred in this region from historical geomagnetic secular variation (Fig. 2c) may be a transient. This interpretation is supported by changes in the instantaneous rotation direction of this vortex[12], occurring between 1840 and 1990.

The thermochemical wind flows efficiently extract heat and light elements from the equatorial belt of the inner boundary (Fig. 2e), while the polar vortex circulations in the tangent cylinder suppress the buoyancy extraction, yielding lower-than-average mass anomaly flux in the polar regions. Our model thus confirms the likelihood of a faster inner-core growth in the equatorial region, in line with earlier predictions[6,23]. It also predicts an extra mass anomaly flux release and locally faster inner-core growth below southeastern Asia, where the sub-Asian cyclone brings colder, chemically depleted material from the outer boundary towards the inner boundary. This maximum coincides with the maximum perturbation in the isotropic seismic velocity of the upper inner core[2] (Fig. 2e), which is also representative of the large-scale pattern of anisotropic[2,3] and first-order attenuation[4] properties. This result is weakly sensitive to the time-average mass anomaly flux partition between the inner and outer boundaries, as shown (Fig. 2f) by a simulation in which the inner-boundary mass anomaly flux is increased from 50% to 80% of the total, to better match current estimates (see Methods).

Solidification texturing appears to be the most likely micromechanism for explaining seismic heterogeneity below the inner core boundary, because the alternative process, deformational texturing, is too slow, typically requiring 1 Gyr timescales[23]. Solidification experiments reveal the importance of interstitial solute flow rate in controlling fabric development in hexagonal-close-packed alloys[24]. Slower freezing rates result in more widely spaced dendritic platelets with greater sensitivity to the solute flow direction, and produce a more textured solid through preferential *c*-axis orientation, whereas faster freezing rates inhibit this effect and result in a solid with more random platelet orientation. Seismic waves that sample the top of the inner core will therefore have anisotropic wave speed and attenuation in the more textured slow-growing regions, and will be more isotropic, faster on average and more attenuated[25] (due to scattering by an increased number of grain boundary crossings) in the less-textured fast-growing regions. If inner core textures are controlled by the processes just described, then the heterogeneous crystallization predicted by our dynamo model qualitatively agrees with the ensemble of seismic data[25]. Our results therefore strongly suggest that the upper inner core has inherited its seismic heterogeneity through mantle-induced lateral variations in its growth rate.

Our interpretation requires a small inner core rotation with respect to the lower mantle over the past 100–300 Myr. Subject to a long term magnetic torque $\bar{\Gamma}_B$, viscous torque $\bar{\Gamma}_v$ and gravitational

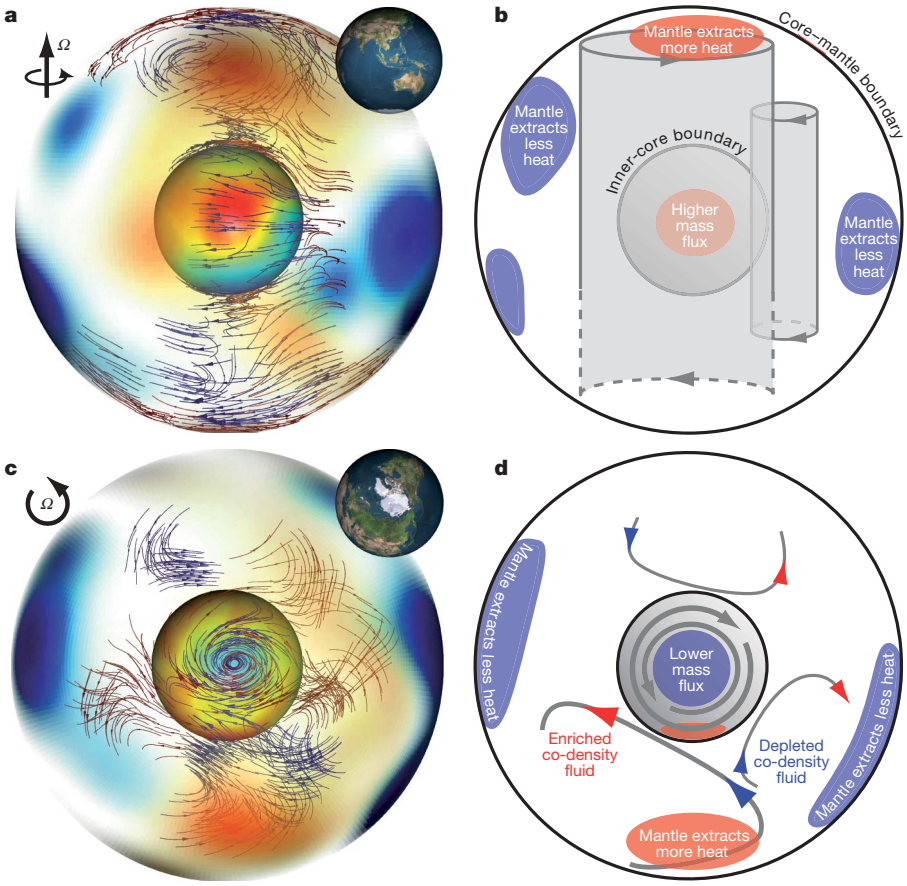

Figure 1 | Time-average flow structure of model case I. Parameters for this case are given in Methods. **a**, **c**, Equatorial and polar visualizations, respectively, of the time-average flow. Insets at upper right indicate the viewing angle. Insets at upper left show the rotation axis direction. The outer boundary is made selectively transparent and colour-coded according to the imposed outwards heat flow (a red patch, such as the dominant positive anomaly below Asia, means a larger-than-average heat flow; see also Supplementary Fig. 1). The inner boundary is colour-coded according to the mass anomaly flux $f = -\kappa\partial C/\partial r$ extracted from the inner core (colour scheme as in Fig. 2e). Within the shell, flow streamlines are represented and colour-coded according to the local velocity along the cylindrical radius (blue streamlines represent downwellings). **b**, **d**, Explanatory diagrams of the equatorial and polar views **a**, **c**. Red and blue arrowheads in **d** respectively represent flow up- and downwellings.

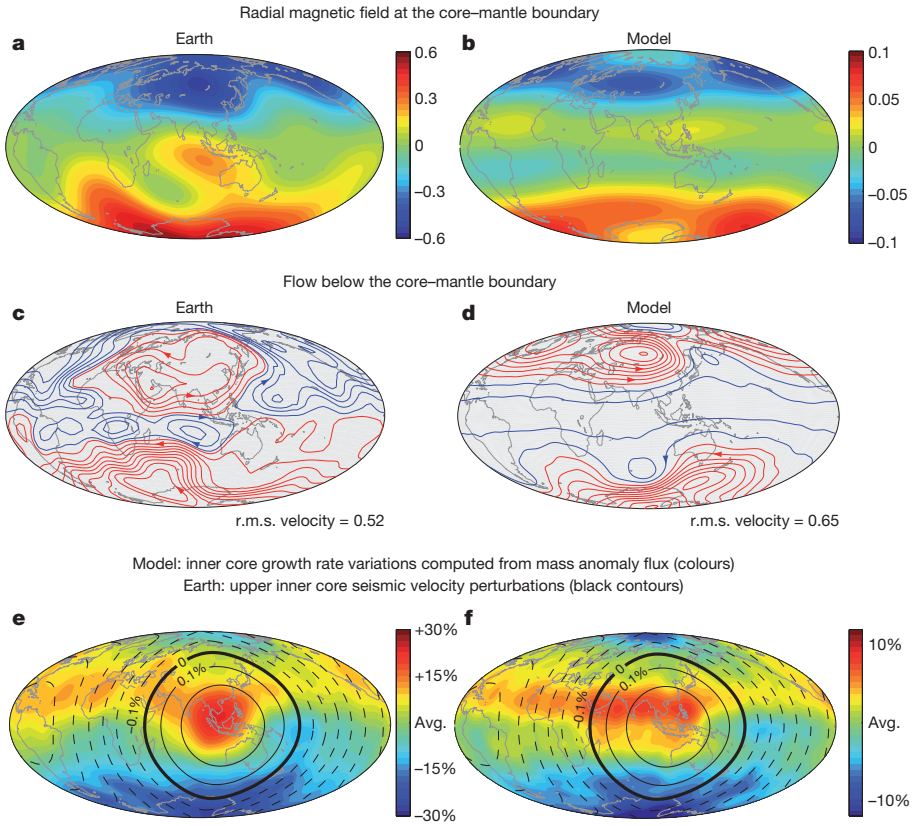

Figure 2 | Comparison between model and observations. a, Time-average palaeomagnetic field model[10] at the core–mantle boundary over the normal polarity periods of the past 5 Myr. **b**, Time-average magnetic field at the outer boundary for case I, taken over the stable polarity periods of 0.7 Myr, and filtered to spherical harmonic degree and order 5. In **a** and **b**, the amplitude (colour scale) is normalized relative to the values predicted by a systematic scaling study[21] (the predicted magnetic field strength in the Earth's core is 1 mT, see Supplementary Information). **c**, Streamlines of the time-average flow below the core–mantle boundary, obtained from geomagnetic secular variation inversions[12], for the period 1840–1990. **d**, Streamlines of the time-average flow at the top of the free stream for case I. In **c** and **d**, the root-mean-squared velocity is normalized relative to the values predicted by thermal wind scaling[11] (the predicted flow amplitude for the core is 15.8 km yr^{-1}, see also Supplementary Information). **e**, Colour map of relative anomalies of the mass anomaly flux extracted from the inner boundary for case I (or, equivalently, of inner-core growth rate anomalies). The black contours show an upper inner core seismic velocity perturbation model[2] expanded to spherical harmonic degree and order 1, the pattern of which is representative of anisotropic[2,3] and attenuation[4] seismic properties. **f**, Same as **e**, for case II (see Methods).

torque with coupling constant Γ_G, the inner core can be expected to reach a steady rotation rate[26] $\bar{\omega} = (\bar{\Gamma}_B + \bar{\Gamma}_v)/\tau\Gamma_G$, where τ is the relaxation time of the inner core towards its hydrostatic shape. The observation[27] of a 6-yr gravitational oscillation in length-of-day data implies that $\tau > 5$ yr and $\Gamma_G = 3 \times 10^{20}$ N m. Numerical dynamo simulations[26] with gravitational coupling further show that in the long term, the system tends to minimize $\bar{\Gamma}_B$, and that when the viscous torque is taken into account, both magnetic and gravitational torques independently counteract the viscous torque which entrains the inner core rotation. These results suggest that $\bar{\Gamma}_B + \bar{\Gamma}_v$ is only a fraction of the typical turbulent viscous torque, which we estimate by assuming a relative zonal flow velocity of the same order of magnitude (10^{-4} m s^{-1}) as at the core surface[12]. Using equation (9) of ref. 28, this yields $\bar{\Gamma}_v = 2 \times 10^{12}$ N m, and a maximum inner core rotation of only 8° in 100 Myr, compatible with our results. On decadal timescales, additional torsional oscillations are expected to disrupt the steady Taylor state of the outer core. For a 60-yr periodicity, magnetic torque fluctuations much larger than $\bar{\Gamma}_B$ can then cause the inner core to oscillate at a maximum angular velocity of[29] 0.1° yr^{-1}, within the range of present seismic inferences[30]. Both processes would only smear, but not erase, the mantle signature on the inner core.

METHODS SUMMARY

We solve for fluid motion, thermochemical transport and magnetic induction in a spherical shell of aspect ratio $r_i/r_o = 0.35$, rotating with constant angular velocity Ω. The non-dimensional Navier–Stokes and induction equations are identical to those presented in an earlier study[11]. The boundary conditions are rigid for the velocity field, and insulating for the magnetic field. The thermochemical buoyancy described by the co-density field C obeys the following evolution equation:

$$\frac{\partial C}{\partial t} + \mathbf{u}\cdot\nabla C = \frac{E}{\mathrm{Pr}}\nabla^2 C + S_T - S_\chi \qquad (1)$$

Here $\mathbf{u}$ is the flow velocity field, and S_T and S_χ are respectively the volumetric thermal buoyancy source and chemical buoyancy sink terms. In model cases I and II, the relevant dimensionless parameters are set as follows: the Ekman number is $E = \nu/\Omega D^2 = 3 \times 10^{-4}$, where $D = r_o - r_i$ is the shell gap and ν is the fluid viscosity. The Prandtl number is $\mathrm{Pr} = \nu/\kappa = 1$, and the magnetic Prandtl number is $\mathrm{Pm} = \nu/\lambda = 2$, where λ is the magnetic diffusivity. The Rayleigh number based on the homogeneous mass anomaly flux[21] f_o imposed at the outer boundary is $\mathrm{Ra}_Q = g_o f_o/\rho\Omega^3 D^2$, where ρ is the fluid density and g_o is the gravity at the outer boundary. Model case I (Figs 1 and 2b, d, e) has $S_T + S_\chi = 0$ and $\mathrm{Ra}_Q = 2 \times 10^{-4}$. Model case II (Fig. 2f) has $S_T + S_\chi = -2.1 \times 10^{-3}$ and $\mathrm{Ra}_Q = 8.1 \times 10^{-5}$.

Full Methods and any associated references are available in the online version of the paper at www.nature.com/nature.

Received 9 November 2007; accepted 12 May 2008.

1. Niu, F. L. & Wen, L. X. Hemispherical variations in seismic velocity at the top of the Earth's inner core. *Nature* **410**, 1081–1084 (2001).
2. Tanaka, S. & Hamaguchi, H. Degree one heterogeneity and hemispherical variation of anisotropy in the inner core from PKP(BC)-PKP(DF) times. *J. Geophys. Res.* **102**, 2925–2938 (1997).
3. Yu, W. C. & Wen, L. X. Inner core attenuation anisotropy. *Earth Planet. Sci. Lett.* **245**, 581–594 (2006).
4. Cao, A. & Romanowicz, B. Hemispherical transition of seismic attenuation at the top of the Earth's inner core. *Earth Planet. Sci. Lett.* **228**, 243–253 (2004).

5. Sumita, I. & Olson, P. A laboratory model for convection in Earth's core driven by a thermally heterogeneous mantle. *Science* **286,** 1547–1549 (1999).
6. Bergman, M. I., Macleod-Silberstein, M., Haskel, M., Chandler, B. & Akpan, N. A laboratory model for solidification of Earth's core. *Phys. Earth Planet. Inter.* **153,** 150–164 (2005).
7. Olson, P. & Christensen, U. The time averaged magnetic field in numerical dynamos with non-uniform boundary heat flow. *Geophys. J. Int.* **151,** 809–823 (2002).
8. Gubbins, D., Willis, A. P. & Sreenivasan, B. Correlation of Earth's magnetic field with lower mantle thermal and seismic structure. *Phys. Earth Planet. Inter.* **162,** 256–260 (2007).
9. Johnson, C. L. & Constable, C. G. The time averaged geomagnetic field as recorded by lava flows over the past 5 Myr. *Geophys. J. Int.* **122,** 489–519 (1995).
10. Kelly, P. & Gubbins, D. The geomagnetic field over the past 5 million years. *Geophys. J. Int.* **128,** 315–330 (1997).
11. Aubert, J., Amit, H. & Hulot, G. Detecting thermal boundary control in surface flows from numerical dynamos. *Phys. Earth Planet. Inter.* **160,** 143–156 (2007).
12. Amit, H. & Olson, P. Time average and time dependent parts of core flow. *Phys. Earth Planet. Inter.* **155,** 120–139 (2006).
13. Lay, T., Hernlund, J., Garnero, E. J. & Thorne, M. S. A post-perovskite lens and D'' heat flux beneath the central Pacific. *Science* **314,** 1272–1276 (2006).
14. van der Hilst, R. *et al.* Seismostratigraphy and thermal structure of Earth's core-mantle boundary region. *Science* **315,** 1813–1817 (2007).
15. Masters, G., Laske, G., Bolton, H. & Dziewonski, A. in *Earth's Deep Interior: Mineral Physics and Tomography from the Atomic to the Global Scale* (eds Karato, S., Forte, A., Liebermann, R. C., Masters, G. & Stixrude, L.) 63–87 (AGU Monogr. Vol. 117, American Geophysical Union, Washington DC, 2000).
16. van der Hilst, R., Widiyantoro, S. & Engdahl, E. R. Evidence for deep mantle circulation from global tomography. *Nature* **386,** 578–584 (1997).
17. McNamara, A. K. & Zhong, S. J. Thermochemical structures beneath Africa and the Pacific Ocean. *Nature* **437,** 1136–1139 (2005).
18. Torsvik, T. H., Smethurst, M. A., Burke, K. & Steinberger, B. Large igneous provinces generated from the margins of the large low-velocity provinces in the deep mantle. *Geophys. J. Int.* **167,** 1447–1460 (2006).
19. Labrosse, S., Poirier, J. P. & Le Mouel, J. L. The age of the inner core. *Earth Planet. Sci. Lett.* **190,** 111–123 (2001).
20. Braginsky, S. I. & Roberts, P. H. Equations governing convection in Earth's core and the geodynamo. *Geophys. Astrophys. Fluid Dyn.* **79,** 1–97 (1995).
21. Christensen, U. & Aubert, J. Scaling properties of convection-driven dynamos in rotating spherical shells and application to planetary magnetic fields. *Geophys. J. Int.* **117,** 97–114 (2006).
22. Olson, P., Christensen, U. & Glatzmaier, G. A. Numerical modelling of the geodynamo: Mechanisms of field generation and equilibration. *J. Geophys. Res.* **104,** 10383–10404 (1999).
23. Yoshida, S., Sumita, I. & Kumazawa, M. Growth model of the inner core coupled with the outer core dynamics and the resulting elastic anisotropy. *J. Geophys. Res.* **101,** 28085–28103 (1996).
24. Bergman, M. I., Agrawal, S., Carter, M. & Macleod-Silberstein, M. Transverse solidification textures in hexagonal close-packed alloys. *J. Cryst. Growth* **255,** 204–211 (2003).
25. Cormier, V. Texture of the uppermost inner core from forward and back scattered seismic waves. *Earth Planet. Sci. Lett.* **258,** 442–453 (2007).
26. Buffett, B. A. & Glatzmaier, G. A. Gravitational braking of inner-core rotation in geodynamo simulations. *Geophys. Res. Lett.* **27,** 3125–3128 (2000).
27. Mound, J. E. & Buffett, B. A. Detection of a gravitational oscillation in length-of-day. *Earth Planet. Sci. Lett.* **243,** 383–389 (2006).
28. Aurnou, J. & Olson, P. Control of inner core rotation by electromagnetic, gravitational and mechanical torques. *Phys. Earth Planet. Inter.* **117,** 111–121 (2000).
29. Dumberry, M. Geodynamic constraints on the steady and time-dependent inner core axial rotation. *Geophys. J. Int.* **170,** 886–895 (2007).
30. Souriau, A. in *Treatise on Geophysics* Vol. 1, *Seismology and Structure of the Earth* (eds Dziewonski, A. & Romanowicz, B.) 655–693 (Elsevier, 2007).

Supplementary Information is linked to the online version of the paper at www.nature.com/nature.

Acknowledgements J.A. was supported by the SEDIT programme of CNRS-INSU. H.A. was supported by a Marie Curie intra-European grant. Numerical calculations were performed at the Service de Calcul Parallèle, IPGP, and at IDRIS, France. We thank S. Tanaka for providing published data, and V. Cormier for discussions. This is IPGP contribution 2369.

Author Information Reprints and permissions information is available at www.nature.com/reprints. Correspondence and requests for materials should be addressed to J.A. (aubert@ipgp.jussieu.fr).

METHODS

We consider an electrically conducting, incompressible fluid in a spherical shell between radii r_i and r_o. The aspect ratio is $r_i/r_o = 0.35$, as in the Earth's core. The shell is rotating about an axis $\mathbf{e}_z$ with constant angular velocity Ω. We model thermal and chemical convection in the Boussinesq approximation, and define the deviation temperature field T' and light element molar fraction field χ' with respect to the adiabatic temperature and well-mixed molar fraction. Both buoyancy effects are grouped into a co-density (or density anomaly) field[20] C such that:

$$C = \alpha\rho T' + \Delta\rho\chi' \quad (1)$$

Here α is the thermal expansion coefficient, ρ is the fluid density, and $\Delta\rho$ is the density difference between light elements and pure iron. The temperature and molar fraction fields are assumed to have the same diffusivity κ, due to turbulent mixing in the outer core. This allows us to write a single transport equation for the co-density C, which is solved numerically in a non-dimensional form, together with the magnetic induction equation for the solenoidal magnetic field $\mathbf{B}$ in the magnetohydrodynamic approximation, and the Navier–Stokes and thermochemical transport equations for the incompressible velocity field $\mathbf{u}$, and pressure P:

$$\frac{\partial\mathbf{u}}{\partial t} + \mathbf{u}\cdot\nabla\mathbf{u} + 2\,\mathbf{e}_z\times\mathbf{u} + \nabla P = \mathrm{Ra}_Q\frac{\mathbf{r}}{r_o}C + (\nabla\times\mathbf{B})\times\mathbf{B} + E\nabla^2\mathbf{u} \quad (2)$$

$$\frac{\partial\mathbf{B}}{\partial t} = \nabla\times(\mathbf{u}\times\mathbf{B}) + \frac{E}{\mathrm{Pm}}\nabla^2\mathbf{B} \quad (3)$$

$$\frac{\partial C}{\partial t} + \mathbf{u}\cdot\nabla C = \frac{E}{\mathrm{Pr}}\nabla^2 C + S_T - S_\chi \quad (4)$$

$$\nabla\cdot\mathbf{u} = 0 \quad (5)$$

$$\nabla\cdot\mathbf{B} = 0 \quad (6)$$

Time is scaled with the inverse of the rotation rate Ω^{-1}. Length is scaled with the shell gap $D = r_o - r_i$. The velocity is scaled with ΩD. The magnetic induction is scaled with $(\rho\mu)^{1/2}\Omega D$, where μ is the magnetic permeability of the fluid. The co-density is scaled with $|f_o|/\Omega D$, where f_o is the amplitude of the spherically symmetric part of the mass anomaly flux $\mathbf{f} = -\kappa\nabla C$ imposed at the outer boundary of the model.

At both boundaries, the boundary conditions for velocity are rigid, and insulating for the magnetic field. Although treating the inner core as an insulator is non-physical, the influence of inner-core conductivity is insignificant[31], except for inner-core differential rotation, which is however not allowed in the present simulations.

At the outer boundary of the model, the mass anomaly flux is prescribed with an homogeneous part f_o and an heterogeneous part proportional to the lower mantle seismic shear wave tomography[15] SB4L18 (see Supplementary Fig. 1), truncated at spherical harmonic degree and order 9, and scaled to have a peak-to-peak magnitude of $\delta f = f_o$. At the inner boundary, the co-density is fixed (see Supplementary Information for a justification of this condition).

The Ekman number is $E = \nu/\Omega D^2 = 3\times10^{-4}$, where ν is the fluid viscosity. The Prandtl number is $\mathrm{Pr} = \nu/\kappa = 1$, and the magnetic Prandtl number is $\mathrm{Pm} = \nu/\lambda = 2$, where λ is the magnetic diffusivity. The Rayleigh number based on mass anomaly flux[21] is $\mathrm{Ra}_Q = g_o f_o/\rho\Omega^3 D^2$, where g_o is the gravity at the outer boundary. In equation (4), S_T is a source term representing the cooling over time of the reference adiabatic thermal state, and S_χ is a sink term representing the enrichment over time of the reference chemical state. Adjusting $S_T + S_\chi$ influences the relative strength of the inner-boundary and outer-boundary originated mass anomaly fluxes on time average. Simulations are carried out for two cases with approximately equal convective power: case I (Figs 1 and 2b, d, e), where $S_T + S_\chi = 0$ and $\mathrm{Ra}_Q = 2\times10^{-4}$, for which scaling laws already exist in the literature[11,21], and a geophysically more relevant[32] case II (Fig. 2f) where $S_T + S_\chi = -2.1\times10^{-3}$ and $\mathrm{Ra}_Q = 8.1\times10^{-5}$. In case II, the inner-boundary originated mass anomaly flux represents 80% of the total.

The numerical implementation MAGIC[31] is used in this study. A Chebyshev polynomials expansion is used in the radial direction with 65 radial grid points. A spherical harmonics expansion is used in the lateral directions, up to maximum degree and order 85.

The model is time-averaged during 4.4 magnetic diffusion times D^2/λ. Using $D = 2{,}200$ km and $\lambda \approx 1\ \mathrm{m^2\,s^{-1}}$ for iron in the Earth's core[33], this is equivalent to a period of about 700 kyr. The time-average magnetic field is taken during the run periods of stable dipole.

31. Wicht, J. Inner-core conductivity in numerical dynamo simulations. *Phys. Earth Planet. Inter.* **132**, 281–302 (2002).
32. Lister, J. R. & Buffett, B. A. The strength and efficiency of thermal and compositional convection in the geodynamo. *Phys. Earth Planet. Inter.* **91**, 17–30 (1995).
33. Secco, R. A. & Shloessin, H. H. The electrical resistivity of solid and liquid Fe at pressures up to 7 GPa. *J. Geophys. Res.* **94**, 5887–5894 (1989).